CARDIAC ANATOMY AS A BIOMETRIC

Noel C. F. Codella, Jonathan Connell, Nalini Ratha

IBM T.J. Watson Research Center
Hawthorne, NY
{nccodell, jconnell, ratha}@us.ibm.com

Jonathan W. Weinsaft, M.D.

Weill Cornell Medical College
New York, NY
jww2001@med.cornell.edu

ABSTRACT

In this study, we propose a novel biometric signature for human identification based on anatomically unique structures of the left ventricle of the heart. An algorithm is developed that analyzes the 3 primary anatomical structures of the left ventricle: the endocardium, myocardium, and papillary muscles. Comparisons of these analyses between probe and gallery images produces a similarity score that is used as the basis of the biometric. The performance of the algorithm is tested on a cohort of 10 de-identified subjects imaged by Cardiac MRI. Perfect matching between individuals is obtained with good separation between the genuine and impostor classes. In summary, this study demonstrates using anatomy of the left ventricle of the human heart for the purposes of a biometric signature.

Index Terms— Cardiac, Anatomy, Biometric, Left, Ventricle

1. INTRODUCTION

The demand for robust biometrics is high in today's security conscious society. While biometrics is considered a secure authentication method, there have been several instances where artificial fingerprints [1] have been used to circumvent biometric security systems. In other biometrics modalities, similar attacks are possible, such as face masks to hide identity, and designer iris lenses to fool iris recognition systems.

In order to address these challenges, recent work has been performed to develop biometrics methods based on ECG signals generated by the human heart [2, 3, 4, 5]. The human heart is a vital internal organ that is difficult to modify without grave risk to the health of the individual. ECG signals represent the electrical activity of the heart, resulting from the propagation of action potentials. Biometric uniqueness between individuals comes from a combination of anatomical uniqueness (macroscopic level spatial distribution of cardiac tissues), and electrical uniqueness (microscopic protein forms and expression levels, electrolyte content, autonomic nervous system input). However, the electrical components are particularly vulnerable to variation from changes in electrolytes, nervous system inputs, hormonal signals, pathological states, pharmacological agents, or emotional and psychological changes [6, 7, 8]. Recent studies show that intra-individual variability of ECG signals prevent perfect threshold template matching [2, 9, 8], and that various forms of task induced stress were able to prevent matching [8].

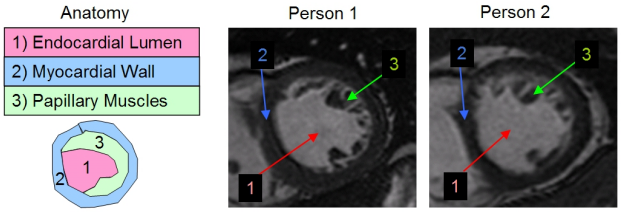

Fig. 1. Layout of the left ventricular anatomy in the short-axis plane of two Cardiac MRI images from separate individuals. The anatomy displays a rich structure that varies considerably between individuals.

We introduce a new biometric using direct anatomical measurements of the left ventricle, which eliminates the intra-individual electrical variability seen with ECG, while preserving biometric uniqueness from complex cardiac structure. Cardiac structure is macroscopic and easy to image using existing technologies. This work is based on one such technique, Cardiac Magnetic Resonance Imaging (MRI). The rich structure of the left ventricle as captured by Cardiac MRI is shown in Figure 1, and has been described to exhibit unique anatomical characteristics across individuals [10, 11].

The rest of this paper is organized as follows: section 2 describes the data collection protocol. Section 3 describes the algorithm. The results and a discussion are presented in sections 4 and 5, respectively. Section 6 concludes.

2. DATA COLLECTION

A short-axis cinematic steady state free-precession (Cine SSFP) magnetic resonance imaging (MRI) technique [12] was used to acquire cardiac image data from 10 randomly

selected de-identified subjects[1] at 2 different times, spanning several months to 2 years, corresponding to gallery enrollment and probe datasets. Cine SSFP images are acquired for multiple slice positions from left ventricular base to apex, and for multiple temporal phases along the cardiac cycle. In-plane image dimensions were 34 cm by 34 cm, with 6 mm slice thickness, and 4 mm spacing between consecutive slices. The end diastolic phase (temporal phase where the left ventricle has filled with its maximal capacity of blood) was selected, and 3 image slices that clearly depict the papillary structures in basal, mid-ventricular, and apical levels were used as biometric signatures.

3. ALGORITHM DEVELOPMENT

In order to facilitate a robust measure of similarity $S(p_x, g_y)$ between individual x in the probe dataset p, and individual y in the gallery dataset g, an algorithm was developed that performs an analysis of the 3 primary anatomical features of the left ventricle: the endocardium, the myocardium, and the papillary muscles. Each analysis produces its own unique similarity score S^E, S^M, and S^P. The final similarity measure S is computed as the average:

$$S(p_x, g_y) = \frac{S^E(p_x, g_y) + S^M(p_x, g_y) + S^P(p_x, g_y)}{3} \quad (1)$$

Since there are 10 individuals in this study, this produces a 10x10 similarity matrix. Each of the 3 analysis techniques will now be described in detail.

3.1. Endocardial Analysis

The endocardial analysis utilizes a previously published clinical segmentation technique named LV-METRIC [13, 14, 15, 16], a soft-segmentation technique that computes the fractional content of blood and myocardium in each voxel comprising the left ventricle, which should be useful for capturing the anatomically complex structure of the endocardium.

Using the endocardial segmentation results, a measure is defined to quantify the anatomical similarity $S^E_{img}(p_{x,z}, g_{y,z})$ between any two cross-sectional images of the left ventricle:

$$S^E_{img}(p_{x,z}, g_{y,z}) = (1 - D_E(p_{x,z}, g_{y,z})) \quad (2)$$

where $p_{x,z}$ corresponds to the z^{th} image of individual x in the probe dataset, and $g_{y,z}$ corresponds to the z^{th} image of individual y in the gallery dataset. The D_E image distance function is defined in Fig. 2a.

Similarity between entire individuals $S^E(p_x, g_y)$ from the probe and gallery datasets are determined by taking the average similarity between each image-level pair-wise comparison:

[1] All personally identifiable information had been removed and were not accessible to the authors of this study, according to section 164.514 of the Health Insurance Portability and Accountability Act (HIPAA).

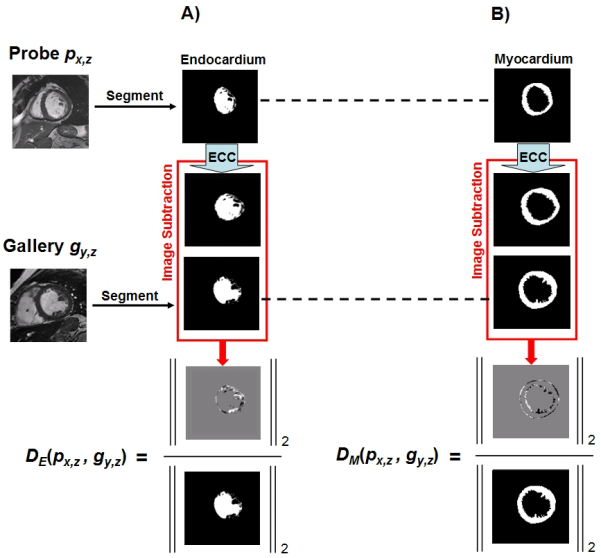

Fig. 2. Anatomical distances are computed by segmentation of both probe and gallery images, registration of the probe to the gallery segmentation, subtraction of the registered segmentations, and finally the L2-norm of the result scaled by the L2-norm of the gallery image. A) Endocardial distance computation. B) Myocardial distance computation.

$$S^E(p_x, g_y) = \frac{1}{N_z} \sum_{z=1}^{N_z} S^E_{img}(p_{x,z}, g_{y,z}) \quad (3)$$

where N_z = 3.

3.2. Myocardial Analysis

The myocardial analysis is based on the LV-ITHACA [15] clinical myocardial segmentation algorithm, which is an active contour model (ACM) technique initialized by the convex hull of the LV-METRIC results. Contour energy is iteratively minimized, defined by a combination of internal forces involving shape stiffness, and external forces involving edge and intensity information, relative to myocardial signal intensity estimated by LV-METRIC.

As in the case of the endocardial analysis, the similarity measure between images $S^M_{img}(p_{x,z}, g_{y,z})$ and similarities between individuals $S^M(p_x, g_y)$ are computed using Eqs. 2 and 3, respectively, replacing D_E with D_M, in Eq. 2 as defined in Fig. 2b, and S^E_{img} with S^M_{img} in Eq. 3.

3.3. Papillary Analysis

The papillary analysis isolates discrete papillary muscles for the purposes of biometric matching. The first step of the analysis finds the left ventricle by enhancing contrast, thresholding the image, then selecting the region nearest the center. A

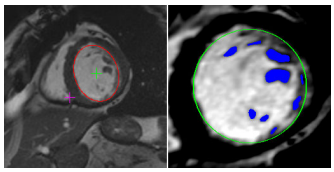

Fig. 3. The interior of the ventricle is approximated with an ellipse (left). This, together with the location of the septum, allows us to normalize the image and find the papillary muscles (right).

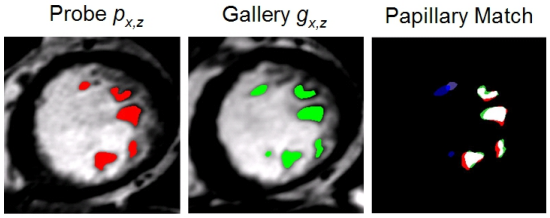

Fig. 4. Papillary matching of probe and gallery images from the same individual. Overlap of more than 50% is considered a perfect match (white), as opposed to a non-match (dark blue), in order to overcome minor registration problems.

centroid and ellipse are then fitted to the left ventricular region, and used to warp the ventricle to a circular shape. The image is then rotated to a normalized orientation based on two points designating the center of the ventricle and the posterior end of the mid-ventricular septum. The point on the septum is located at the lower right corner of the right ventricle, which is detected as the first region to the left of the left ventricle. Finally, the geometrically corrected image is again contrast enhanced. Fig. 3 shows a sample of the elliptical approximation and the localization of the septum (left) which is then used to generate the normalized image (right). The warped circular approximation is shown in green.

The next step extracts the papillary muscles by applying a center-surround operator to the normalized image to account for local brightness variations. The result is thresholded, and the regions that are either very small or occur outside of the left ventricle are removed. The remaining regions are again cleaned-up using morphological operations to yield discrete papillary muscles (blue in Fig. 3).

We then compute the pixel overlap of papillary muscle areas. Fig. 4 shows two normalized images with their detected papillary muscles, and the overlap of the papillary muscle pixels. A probe papillary muscle is considered to *completely* match if it overlaps more than 50% with one or more papillary muscles in the gallery image. The aggregated similarity between probe and gallery images is then defined as:

$$S^P_{img}(p_{x,z_1}, g_{y,z_2}) = \frac{P_{matched}}{P_{total}} \quad (4)$$

where $P_{matched}$ is the number of pixels in the union image of all matched elements from the probe and gallery, and P_{total} is the number of pixels in the union image of all elements (matched or unmatched) from the probe and gallery. To compute similarity between entire individuals:

$$S^P(p_x, g_y) = \arg\max_{z_1,z_2} S^P_{img}(p_{x,z_1}, g_{y,z_2}) \quad (5)$$

where z_1 and z_2 can take on values 1 through 3.

4. RESULTS

Fig. 5 shows the results in the form of a similarity matrix and a similarity histogram. A global threshold of 80 can be used to define a clear and perfect biometric match across the entire population of 10 subjects. Good separation is seen between genuine and impostor matches when examining each row or column of the similarity matrix independently. The average relative separation between genuine and impostor matches was 30.4%, with a standard deviation of 8.7%.

5. DISCUSSION

This work has been the first to isolate the cardiac left ventricular anatomy for the purposes of biometric identification. An algorithm was developed that computes similarity based on the analysis of the 3 primary left ventricular anatomical structures, the endocardium, the myocardium, and the papillary muscles. The combination of all three anatomical analyses produced a perfect biometric match on our cohort of 10 individuals. In addition, there was good separation between genuine and impostor matches, suggesting the technique may continue to be effective for larger datasets.

As compared to ECG based biometrics, cardiac anatomy based biometrics are not subject to intra-individual electrical variations, which have been linked with a reduction in matching accuracy for ECG based biometrics [8]. However, the cardiac anatomy is still subject to change from numerous pathological conditions, such as cardiomyopathy and myocardial infarction. Both will also produce changes in the ECG. Future work should compare anatomy to ECG based biometrics to determine the relative performance.

This study was based on the Magnetic Resonance Imaging modality, which produces high quality images, with robust segmentation algorithms available [13, 14, 15]. Future studies should examine the utility of other imaging modalities, such as echocardiography, which may also be well suited to the task of biometric identification.

6. CONCLUSION

In summary, an algorithm has been presented for comparing the anatomical shape of the left ventricle of the heart for the purposes of biometric identification. A perfect matching has

86.7	55.2	70.3	51.8	71.8	64.4	69.4	77.9	61.0	43.8
61.2	**86.2**	52.9	54.0	60.4	62.1	71.0	48.5	69.9	34.0
68.5	48.6	**82.2**	50.6	54.0	52.1	54.5	62.9	52.3	59.8
56.9	47.8	58.9	**85.4**	48.7	64.1	68.5	57.1	56.0	60.5
64.1	66.1	56.6	45.4	**84.8**	61.5	65.8	62.5	59.2	41.1
66.6	60.1	56.6	61.0	60.2	**90.6**	68.3	58.0	57.6	63.7
47.4	68.6	49.9	58.9	57.9	71.6	**87.6**	48.9	65.3	58.2
70.8	56.4	68.0	58.0	68.9	67.2	59.4	**86.6**	59.7	60.4
57.8	66.6	55.3	57.5	60.9	57.5	64.5	54.8	**83.1**	58.0
64.7	50.8	57.8	58.6	59.6	71.8	71.3	61.3	55.3	**80.9**

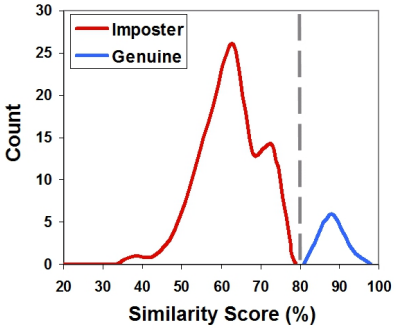

Fig. 5. *Left:* Resulting similarity score table. Rows designate each individual in the gallery, columns designate each individual as a probe. *Right:* Score histogram, showing delineation between genuine and impostor matches at a threshold of 80%.

been achieved in a cohort of 10 individuals with good separation between genuine and impostor matches.

7. REFERENCES

[1] Koji Yamada Satoshi Hoshino Tsutomu Matsumoto, Hiroyuki Matsumoto, "Impact of artificial gummy fingers on fingerprint systems.," *Proceedings of SPIE, Optical Security and Counterfeit Deterrence Techniques*, vol. 8577, October 2002.

[2] Dimitrios Hatzinakos S. Zahra Fatemian, Foteini Agrafioti, "Heartid: Cardiac biometric recognition," *Fourth IEEE International Conference on Biometrics: Theory Applications and Systems*, 2010.

[3] Andrew Cheng Mark Wiederhold Brenda Wiederhold Steven Israel, John Irvine, "Ecg to identify individuals," *Pattern Recognition*, vol. 38, pp. 133–142, 2005.

[4] Gerd Wübbeler, Manuel Stavridis, Dieter Kreiseler, Ralf-Dieter Bousseljot, and Clemens Elster, "Verification of humans using the electrocardiogram," *Pattern Recogn. Lett.*, vol. 28, pp. 1172–1175, July 2007.

[5] Yongjin Wang, Foteini Agrafioti, Dimitrios Hatzinakos, and Konstantinos N. Plataniotis, "Analysis of human electrocardiogram for biometric recognition," *EURASIP J. Adv. Signal Process*, vol. 2008, January 2008.

[6] Majid Haghjoo Mehdy Dousty, Sabalan Daneshvar, "The effects of sedative music, arousal music, and silence on electrocardiography signals," *Journal of Electrocardiology*, vol. 44, pp. 396, 2011.

[7] Ira Galin Amit Dande, Amrita Pandit, "Takotsubo cardiomyopathy followed by neurogenic stunned myocardium in the same patient: Gradations of the same disease," *Cardiology*, vol. 118, no. 3, 2011.

[8] Andrew Cheng Mark Weiderhold Brenda Weiderhold Steven Israel, John Irvine, "Ecg to identify individuals," *Pattern Recognition*, vol. 38, pp. 133–142, 2005.

[9] Shrikanth Narayunan Ming Li, "Robust ecg biometrics by fusing temporal and cepstral information," *International Conference on Pattern Recognition*, 2010.

[10] Robert Howden Henry Gray, T. Pickering Pick, "Gray's anatomy," .

[11] Michael Ross Yi Wang Noel Codella James Min Martin Prince Shant Manoushagian Peter Okin Richard Devereux Jonathan Weinsaft Matthew Janik, Matthew Cham, "Effects of papillary muscles and trabeculae on left ventricular quantification: increased impact of methodological variability in patients with left ventricular hypertrophy," *Hypertension*, vol. 26, pp. 1677–1685, 2008.

[12] Zhu XP Love HG Isherwood I Rowlands DJ Waterton JC, Jenkins JP, "Magnetic resonance (mr) cine imaging of the human heart.," *Br J Radiol.*, vol. 58, no. 692, pp. 711–716, 1985.

[13] Matthew Cham Matthew Janik Martin Prince Yi Wang Noel Codella, Jonathan Weinsaft, "Left ventricle: automated segmentation by using myocardial effusion threshold reduction and intravoxel computation at mr imaging," *Radiology*, vol. 248, no. 3, pp. 1004–1012, 2008.

[14] Richard Wong Christopher Chu James Min Martin Prince Yi Wang Jonathan Weinsaft Noel Codella, Matthew Cham, "Rapid and accurate left ventricular chamber quantification using a novel cmr segmentation algorithm: a clinical validation study," *J Magn Reson Imaging*, vol. 31, no. 4, pp. 845–853, 2010.

[15] Matthew Cham Jonathan Weinsaft Yi Wang Hae-Yeoun Lee, Noel Codella, "Automatic left ventricle segmentation using iterative thresholding and an active contour model with adaptation on short-axis cardiac mri," *IEEE Trans Biomed Eng*, vol. 57, no. 4, pp. 905–913.

[16] Noel Codella, Hae-Yeoun Lee, David Fieno, Debbie Chen, Sandra Hurtado-Rua, Minisha Kochar, John-Paul Finn, Robert Judd, Parag Goyal, Jesse Schenendorf, Matthew Cham, Richard Devereux, Martin Prince, Yi Wang, and Jonathan Weinsaft, "Improved left ventricular quantification with partial voxel interpolation, in vivo and necropsy validation of a novel cardiac mri segmentation algorithm," *Circulation Cardiovascular Imaging*, 2011.